BMC Musculoskeletal Disorders

RESEARCH

Open Access

Three-dimensional architecture characteristics and diffusion properties of masticatory muscles assessed with diffusion tensor imaging and diffusion spectrum imaging: a pilot study of differences, reproducibility and sensitivity to microenvironment changes

Xiang Lin[1,2†], Wei Guo[1,2†], Dejun She[1,2], Jianping Hu[1,2], Hongpeng Dai[1,2], Yang Song[3] and Dairong Cao[1,2,4,5*]

Abstract

Background Diffusion spectral imaging (DSI) could overcome the inherent limitation of diffusion tensor imaging (DTI), but its outcomes in masticatory muscle fiber-tracking have not been well-established. Therefore, the objective of this prospective study conducted in China was to evaluate and compare the performance of DTI and DSI in human masticatory muscles.

Methods The differences and reproducibility of architecture characteristics and diffusion properties derived from DTI and DSI were evaluated in the masticatory muscles of healthy volunteers ($n=25$). The quality of tracked fiber was analyzed based on anatomical information. To assess the sensitivity of DTI and DSI to muscular microenvironment changes, the architecture characteristics and diffusion properties of the masticatory muscles in patients with temporomandibular joint disorders (TMDs) ($n=25$) between different subgroups according to the course of diseases were explored. The paired-samples *t*-test or Wilcoxon signed-rank test, Student's t-test or Mann-Whitney U test, one-way ANOVA or the Kruskal-Wallis test, and the *post-hoc* multiple comparisons with false discovery rate adjustment were performed. Bland-Altman plots, within-subject coefficient of variation (CV), and relative absolute difference (RAD) were used to evaluate the reproducibility.

Results In the healthy group, DSI generated significantly more fibers in all masticatory muscles (all $P<0.001$) and fewer low-quality fibers in most masticatory muscles ($P<0.050$) than DTI did. Moreover, higher values of mean diffusivity (MD), axial diffusivity (AD), and radial diffusivity (RD) were found in DSI (all $P<0.001$). Satisfactory coefficient of variation (< 10%), relative absolute difference (< 10%), and agreement exhibited by the Bland-Altman analysis were

†Xiang Lin and Wei Guo equally contributed to this study.

*Correspondence:
Dairong Cao
dairongcao@163.com

Full list of author information is available at the end of the article

found between two scans in both DTI and DSI. Compared with DTI, DSI found additional significant changes in the masticatory muscles of TMDs patients.

Conclusions Although both DTI and DSI allowed reproducible assessment of masticatory muscles, significant differences existed between them. DSI was more sensitive to the microenvironment changes of the masticatory muscles in TMDs patients.

Keywords Diffusion tensor imaging, Diffusion spectrum imaging, Masticatory muscles, Reproducibility, Temporomandibular joint disorders

Background

Masticatory muscles, the primary anatomical components responsible for mastication, exhibit a complex architecture with a multipennate structure [1–3]. Morphological changes and microstructural impairments in these muscles are closely associated with masticatory dysfunction in humans, resulting in temporomandibular joint disorders (TMDs) or maxillofacial pain [4, 5]. TMDs affect up to 34% of the general population [6], regarded as the most common oral and facial pain condition [7]. Consequently, an accurate assessment of the pathophysiological status of these muscles is crucial for enhancing our understanding of the etiology and severity of these diseases. Furthermore, the effectiveness of TMDs therapies may be associated with the disease course. Previous studies demonstrated early treatment could improve the outcomes and prevent irreversible injury or decelerate its progression [8, 9]. Therefore, a timely and accurate description of the morphology and microstructure of masticatory muscles is of great clinical value.

Currently, clinical diagnosis of TMDs relies on a combination of patient history, physical examination, imaging, and even the assistance of the machine learning algorithm [10, 11]. While conventional magnetic resonance imaging (MRI) has become an increasingly powerful tool for diagnosing TMDs, it can only detect gross structural changes and lacks sensitivity to early microstructural alterations of the masticatory muscles [12]. In the last decade, diffusion tensor imaging (DTI) has gained increasing popularity as a non-invasive method to characterize the morphological features and internal architectural arrangement of the masticatory muscles [13, 14]. Moreover, DTI can detect musculoskeletal changes in earlier stages of the disorders compared to conventional MRI techniques [15]. However, DTI also presents some limitations, including model assumption and relatively low direction resolution (three main directions), which make it insufficient to reveal the complex pathological state and multipennate fiber-bundle structure of masticatory muscles [16–18].

It is well-recognized that diffusion spectrum imaging (DSI) can resolve multiple individual diffusion vectors per voxel thanks to advanced data-acquisition techniques and excellent angular resolution; whereas DTI can only provide a single composite vector per voxel [19]. Recent attempts to employ DSI in muscle imaging have demonstrated its promising ability to resolve complex fiber anatomy [20–22]. Despite these promising findings, the role of DSI in masticatory muscle evaluation remains to be further determined, and comparisons between the results of DTI and DSI in the assessment of these muscles have not been fully explored. More critically, the results of these comparisons may help select the appropriate technique to optimize the microstructural assessment of masticatory muscles and enhance their evaluation.

Thus, this prospective study aimed to evaluate and compare the performance of DTI and DSI in human masticatory muscles, in terms of differences, reproducibility, and sensitivity to muscular microenvironment changes. We hypothesized that DSI may provide different and preferable results of masticatory muscle microstructural characterization.

Methods

The study was approved by the Institutional Review Board of the First Affiliated Hospital of Fujian Medical University (MRCTA, ECFAH of FMU [2021] 674), and written informed consent was obtained from each participant.

Participants

Between January 2023 and January 2024, 25 healthy volunteers were prospectively enrolled in the study. The inclusion criteria for the healthy volunteers were: (1) with no history of maxillofacial muscle injury or disease, (2) no clinical symptoms of TMDs, and (3) normal occlusion. To assess the sensitivity to muscular microenvironment changes, 25 patients with TMDs were also collected. The Diagnostic criteria for temporomandibular disorders (DC/TMD) for clinical and research applications as recommended by the International Original Research Diagnostic Criteria for TMD (DC/TMD) Consortium Network and Orofacial Pain Special Interest Group was applied [23]. The inclusion criteria for patients with TMDs were as follows: (1) pain in the temporomandibular region, (2) joint clicking, popping, and/or snapping noise during jaw movements, (3) maximum assisted opening (passive stretch) movement, including

vertical incisal overlap, < 40 mm and (4) no head or neck treatment before MRI examination [13].

MRI protocols

All participants were scanned with a 3.0-T MRI system (MAGNETOM Prisma, Siemens Healthcare, Erlangen, Germany) using a 64-channel combined head-and-neck coil. The masticatory muscle images were acquired using the following sequences: three-dimensional multiple echo-time T1-weighted volume-interpolated breath-hold examination sequence with Dixon-based water-fat separation for anatomical reference; axial DTI and DSI with single spin-echo refocusing for fiber architecture reconstructions; and b0 maps with reversed phase-encoding polarities for correction of susceptibility-induced distortion. The imaging parameters of the reversed b0 maps aligned with the respective DTI or DSI sequences, except for variations in the b-value and phase-encoding direction. Additionally, the oblique-sagittal and coronal proton density-weighted fast spin echo with fat saturation and T1-weighted fast spin-echo were performed in the closed and open mouth positions in the TMDs group. The details of the MRI protocols are presented in Table S1. The healthy participants were scanned twice within 7 days to assess the reproducibility of DTI and DSI.

Muscle segmentation

Prior to muscle segmentation, co-registration of T1-weighted images (first echo time) with the corresponding acquired b0 maps was performed using the Advanced Normalization Tools software (http://stnava.github.io/ANTs/). Subsequently, the regions of interest were manually drawn on T1-weighted images using ITK-SNAP (Version 3.8.0, http://www.itksnap.org/) by a radiologist specialized in head and neck anatomy (with 6 years of experience in muscle anatomy and geometry assessment). The temporalis muscle was not investigated in this preliminary study, considering the scan time and specific spatial resolution requirement constraints. Therefore, the masticatory muscles were then defined as follows: left and right lateral pterygoid muscles (L- and R-LPM, respectively), left and right medial pterygoid muscles (L- and R-MPM, respectively), and left and right masseter muscles (L- and R-MM, respectively) (Fig. 1).

Diffusion data preprocessing

The geometric deformation caused by noise and eddy currents can substantially impact the image quality; therefore, all diffusion datasets in this study underwent a three-stage preprocessing. First, the raw diffusion data were denoised using the MRtrix3 tool (https://github.com/MRtrix3/mrtrix3). Subsequently, the susceptibility

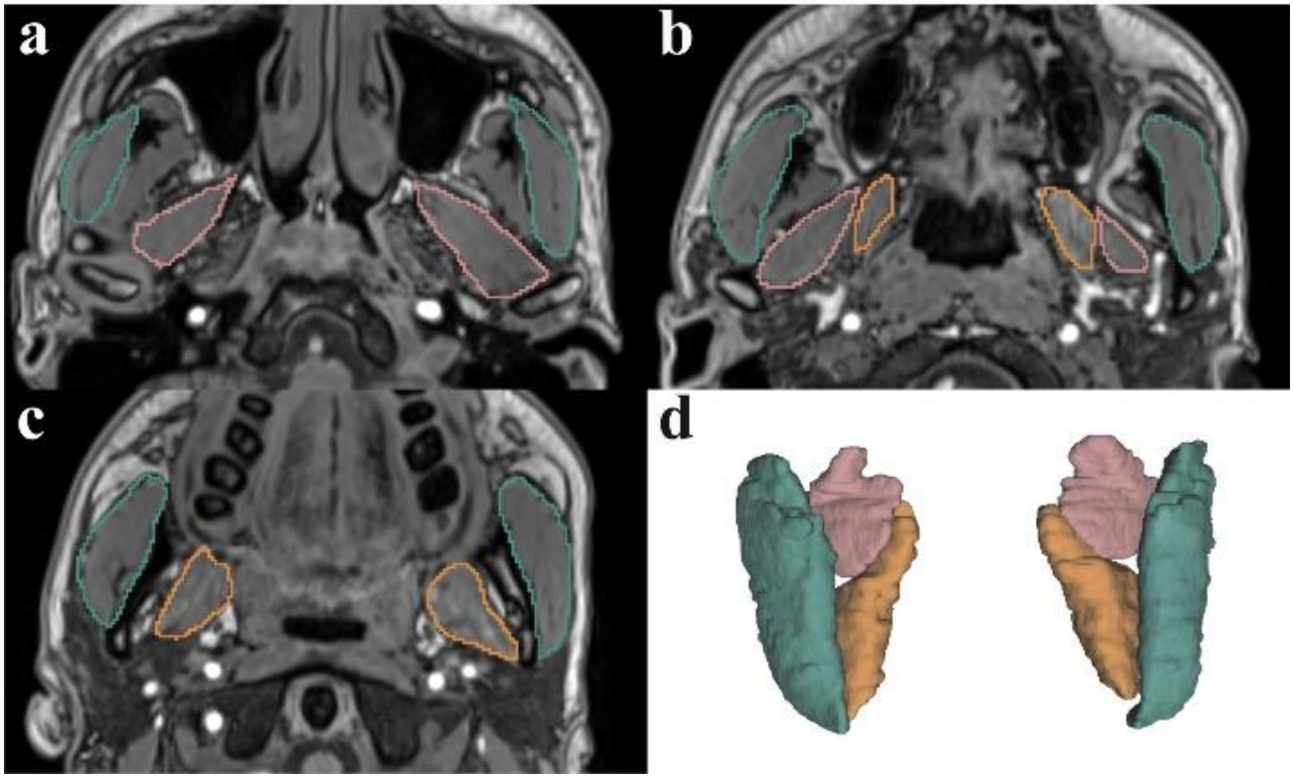

Fig. 1 Masticatory muscle segmentation (**a**, upper plane; **b**, intermediate plane; **c**, lower plane) and three-dimensional volume representation of the regions of interest (**d**)

artifacts were estimated using reversed phase-encoding b0 maps via TOPUP from the Tiny FSL package (http://github.com/frankyeh/TinyFSL). This package represents a recompiled version of the FSL TOPUP (Oxford Centre for Functional MRI of the Brain, Oxford University, Oxford, UK) with multithread support. The susceptibility-induced distortion was corrected using the integrated interface in DSI Studio (http://dsi-studio.labsolver.org). Ultimately, motion correction during data acquisition was automatically implemented using DSI Studio.

Image analysis

Masticatory muscle fiber tracking was performed in DSI Studio using anisotropy and angular thresholds of 0.02 and 30°, respectively [24]. Fibers shorter than 10 mm or longer than 300 mm were excluded. A total of 5,000,000 seeds were drawn for fiber tracking. Before fiber tracking, the registration of T1-weighted images and diffusion data were carefully checked and manually adjusted with DSI Studio if necessary.

In the healthy volunteers, the tracked fibers of the masticatory muscles of each participant were categorized into high- and low-quality fibers. This categorization was based on anatomical knowledge and fiber-processing functions provided by DSI Studio. The low-quality fibers were defined as fibers that extended beyond the muscle boundary by a distance greater than or equal to 5 pixels [25]. Representative results for the total and high- and low-quality fiber classifications are illustrated in Fig. 2.

All patients with TMDs were reviewed by two radiologists (with 6 and 30 years of experience in head and neck MRI diagnosis). According to the status of disc displacement, TMDs patients were categorized into three subgroups: (1) normal disc position (NP), (2) anterior disc displacement with reduction (ADWR), and (3) anterior disc displacement without reduction (ADWOR).

Subsequently, in both healthy volunteers and TMDs patients, the following architecture characteristics and diffusion properties were extracted for each muscle in each participant, including track number (T_N), track mean length (T_{ML}), track volume (T_V), quantitative anisotropy (QA), fractional anisotropy (FA), mean diffusivity (MD), axial diffusivity (AD), and radial diffusivity (RD).

Statistical analysis

The following measures for each masticatory muscle were compared between the two diffusion techniques in each healthy volunteer: (1) percentage of low-quality fibers within the total number of fibers for each muscle; (2) architecture characteristics and diffusion properties, including T_N, T_{ML}, T_V FA, MD, AD, and RD, obtained from the DTI and DSI datasets; and (3) reproducibility of the architecture characteristics and diffusion properties between the two scans of each sequence, for each muscle. The architecture characteristics and diffusion properties were compared between healthy and TMDs groups, and among TMDs subgroups defined by the status of disc displacement. The reproducibility analysis included all

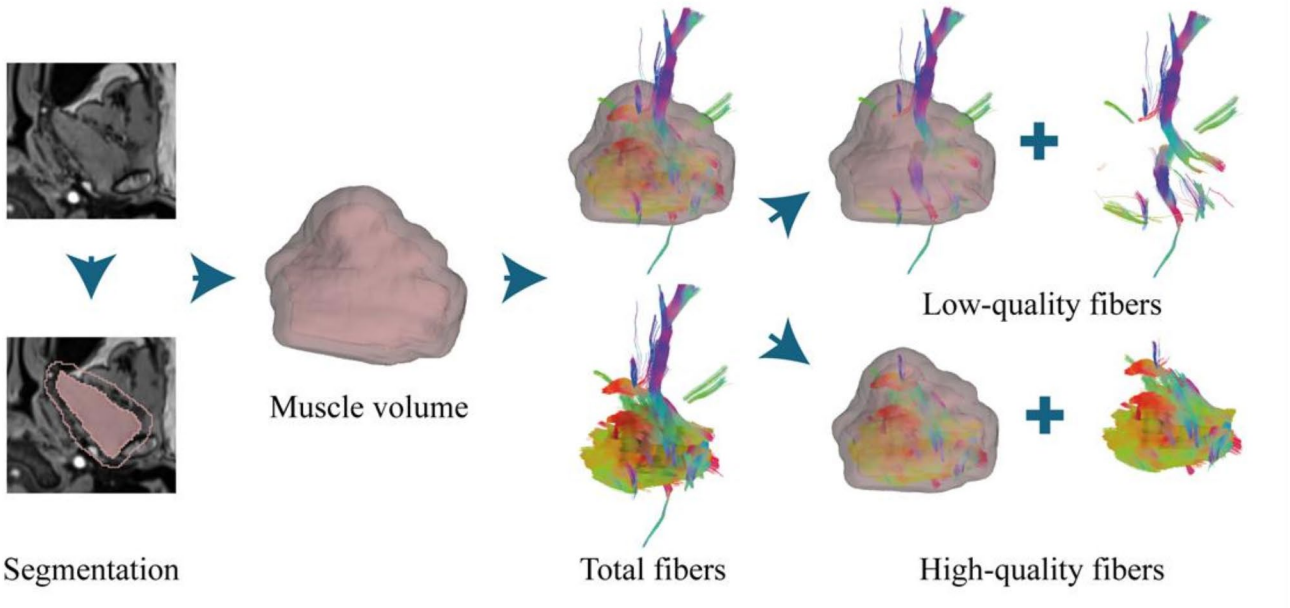

Fig. 2 Low- and high-quality fiber identification. Identification of fibers that extended beyond the muscle boundary by a distance greater than or equal to 5 pixels, which may be caused by the artifacts and incorrect tracking process. The pink area indicated the region of masticatory muscle, and the peripheral line illustrated the limiting boundary

fibers. And other comparisons were limited to the architecture characteristics and diffusion properties of the high-quality fibers to avoid the influence of the incorrect fibers on the results of the masticatory muscle fiber analysis and to facilitate the clinical application.

All statistical analyses were performed using the online application software SPSSAU (version 23.0; https://www.spssau.com, SPSSAU, Haidian, China), and GraphPad Prism 9 (version 9.0.0, https://www.graphpad.com/). The Shapiro-Wilk test was used to analyze the data distribution. Differences with $P<0.05$ were considered statistically significant. The differences between the two diffusion sequences were evaluated using either the paired-samples *t*-test or the Wilcoxon signed-rank test, as appropriate. The reproducibility of the two sequences was assessed with Bland-Altman plots, within-subject coefficient of variation (CV) [26], and relative absolute difference (RAD). The Bland-Altman plots were obtained with the Origin software (Version 2023b; https://www.originlab.com, Origin Lab, Northampton, MA, USA). The CV was calculated as the ratio of the standard deviation of the paired differences to the mean and a CV value < 10% was considered indicative of good reproducibility. The RAD was calculated as follows [27]:

$$RAD = \frac{first\ metric - second\ metric}{(first\ metric + second\ metric) \div 2} \times 100\%$$

The difference between healthy and TMDs groups was analyzed with Student's t-test or Mann-Whitney U test, or Chi-square test, as appropriate. The differences among TMDs subgroups were evaluated with one-way ANOVA or the Kruskal-Wallis test. The *Post-hoc* multiple comparisons with false discovery rate adjustment were employed to further explore the difference between TMDs subgroups.

Results

Initially, 25 healthy volunteers and 25 TMDs patients were included in our study. However, one healthy volunteer did not undergo the second scan, and for another healthy volunteer, the MRI data for one of the scans were insufficient. Therefore, the sample size was reduced to 23 for the evaluation of the DTI and DSI reproducibility.

Comparison between DTI and DSI

The percentage of low-quality fibers was significantly lower in DSI in all masticatory muscles, except for the LPMs (all $P<0.05$ [paired-samples t-test]) (Table S2, Fig. 3). In contrast, in the later muscles, DTI and DSI yielded similar results ($P=0.548$[paired-samples t-test] for the L-LPM, $P=0.353$ [paired-samples t-test] for the R-LPM).

Regarding the architecture characteristics, DSI tracked significantly more fibers in each muscle than DTI (all $P<0.001$ [paired-samples t-test and Wilcoxon signed-rank test]) (Table 1). The T_{ML} obtained with DSI was also significantly shorter in the R-LPM and bilateral MMs (all $P<0.05$ [paired-samples t-test and Wilcoxon signed-rank test]). Furthermore, smaller T_V values were observed with DSI in the bilateral MMs ($P<0.01$ [paired-samples t-test]). As for the diffusion properties, the values of MD, AD, and RD were consistently higher in DSI compared with DTI data (all $P<0.001$ [paired-samples t-test]).

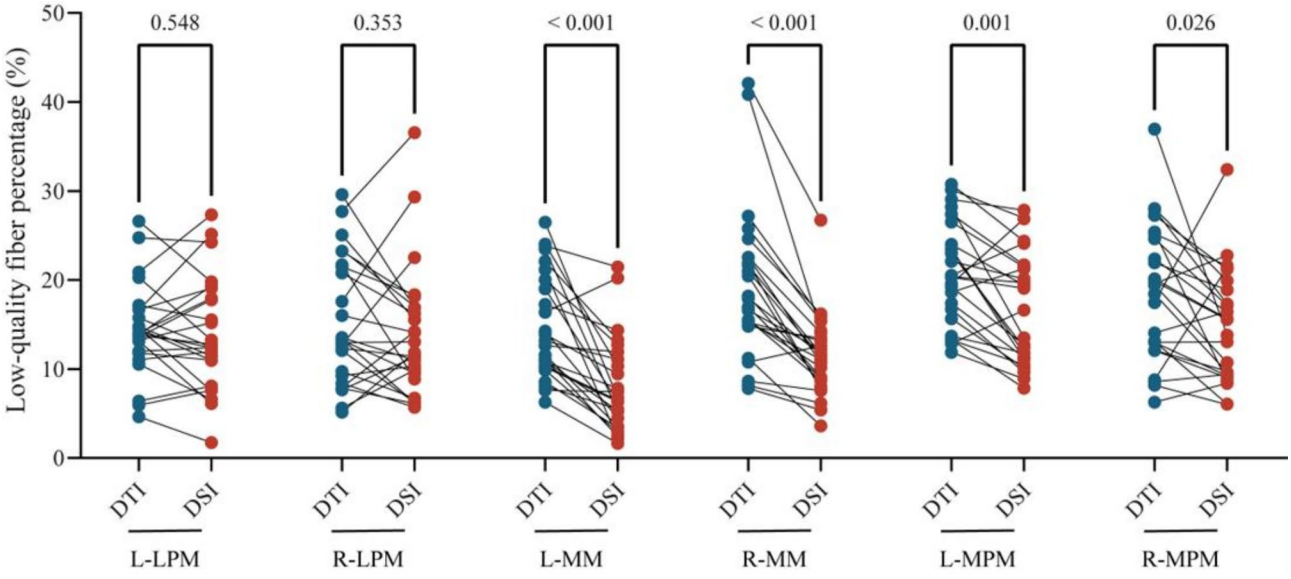

Fig. 3 Paired comparison between the percentage of low-quality fibers tracked with DTI and DSI in each masticatory muscle. L-LPM, left lateral pterygoid muscle; R-LPM, right lateral pterygoid muscle; L-MM, left masseter muscle; R-MM, right masseter muscle; L-MPM, left medial pterygoid muscle; R-MPM, right medial pterygoid muscle; DTI, diffusion tensor imaging; DSI, diffusion spectral imaging

Table 1 Comparison of architecture characteristics and diffusion properties between DTI and DSI

Tract name	Metrics	Left side			Right side		
		DTI ($n=25$)	DSI ($n=25$)	*P*-value	DTI ($n=25$)	DSI ($n=25$)	*P*-value
LPM	T_N ($\times10^3$)	5.14 ± 1.17	19.13 ± 4.61	**< 0.001**[a]	5.43 [4.67, 5.79]	18.39 [16.59, 23.43]	**< 0.001**[b]
	T_{ML} (mm)	20.79 ± 1.59	19.92 ± 3.04	0.103 [a]	22.64 ± 2.30	20.57 ± 2.62	**< 0.001**[a]
	T_V ($\times10^3$ mm^3)	10.29 ± 2.12	10.32 ± 2.15	0.924 [a]	10.56 ± 1.73	10.77 ± 2.19	0.421 [a]
	FA	0.27 [0.25, 0.27]	0.26 [0.25, 0.28]	0.221 [b]	0.27 ± 0.02	0.26 ± 0.02	0.290 [a]
	MD ($\times10^{-3}$ mm^2/s)	1.70 ± 0.16	2.29 ± 0.19	**< 0.001**[a]	1.69 ± 0.15	2.29 ± 0.25	**< 0.001**[a]
	AD ($\times10^{-3}$ mm^2/s)	2.14 ± 0.21	2.92 ± 0.22	**< 0.001**[a]	2.15 ± 0.19	2.92 ± 0.29	**< 0.001**[a]
	RD ($\times10^{-3}$ mm^2/s)	1.47 ± 0.14	1.97 ± 0.18	**< 0.001**[a]	1.46 ± 0.13	1.97 ± 0.23	**< 0.001**[a]
MM	T_N ($\times10^3$)	24.03 ± 6.05	96.24 ± 21.42	**< 0.001**[a]	23.22 ± 5.50	93.52 ± 21.10	**< 0.001**[a]
	T_{ML} (mm)	29.50 [28.09, 32.39]	27.44 [24.14, 33.17]	**0.009**[b]	33.57 [30.92, 35.73]	30.66 [29.07, 34.43]	**0.014**[b]
	T_V ($\times10^3$ mm^3)	38.78 ± 9.17	37.27 ± 8.45	**0.007**[a]	37.14 ± 7.76	35.52 ± 7.72	**0.001**[a]
	FA	0.27 ± 0.02	0.27 ± 0.03	0.391 [a]	0.27 ± 0.02	0.26 ± 0.03	0.149 [a]
	MD ($\times10^{-3}$ mm^2/s)	1.61 ± 0.10	1.82 ± 0.15	**< 0.001**[a]	1.61 ± 0.08	1.82 ± 0.15	**< 0.001**[a]
	AD ($\times10^{-3}$ mm^2/s)	2.07 ± 0.12	2.34 ± 0.15	**< 0.001**[a]	2.06 ± 0.09	2.33 ± 0.15	**< 0.001**[a]
	RD ($\times10^{-3}$ mm^2/s)	1.38 ± 0.09	1.56 ± 0.15	**< 0.001**[a]	1.38 ± 0.08	1.56 ± 0.15	**< 0.001**[a]
MPM	T_N ($\times10^3$)	6.52 ± 1.45	25.78 ± 5.83	**< 0.001**[a]	6.76 ± 1.84	24.13 ± 6.24	**< 0.001**[a]
	T_{ML} (mm)	22.59 ± 2.55	21.51 ± 2.78	0.071 [a]	22.89 ± 3.62	21.17 ± 3.36	0.050 [a]
	T_V ($\times10^3$ mm^3)	12.64 ± 2.57	13.23 ± 3.04	0.069 [a]	12.87 ± 2.89	12.66 ± 3.39	0.485 [a]
	FA	0.27 ± 0.02	0.26 ± 0.02	0.104 [a]	0.26 ± 0.02	0.26 ± 0.02	0.150 [a]
	MD ($\times10^{-3}$ mm^2/s)	1.56 ± 0.10	1.96 ± 0.14	**< 0.001**[a]	1.59 ± 0.11	1.98 ± 0.16	**< 0.001**[a]
	AD ($\times10^{-3}$ mm^2/s)	1.99 ± 0.14	2.49 ± 0.17	**< 0.001**[a]	2.02 ± 0.13	2.51 ± 0.19	**< 0.001**[a]
	RD ($\times10^{-3}$ mm^2/s)	1.35 ± 0.09	1.69 ± 0.13	**< 0.001**[a]	1.37 ± 0.10	1.71 ± 0.15	**< 0.001**[a]

Note: L-LPM, left lateral pterygoid muscle; R-LPM, right lateral pterygoid muscle; L-MM, left masseter muscle; R-MM, right masseter muscle; L-MPM, left medial pterygoid muscle; R-MPM, right medial pterygoid muscle; T_N, track number; T_{ML}, track mean length; T_V, track volume; FA, fractional anisotropy; MD, mean diffusivity; AD, axial diffusivity; RD, radial diffusivity; DTI, diffusion tensor imaging; DSI, diffusion spectral imaging

Bold type indicated $P < 0.05$. The superscript letter "a" indicates the use of the paired-samples t-test, while the superscript letter "b" denotes the use of the Wilcoxon signed-rank test

However, no significant difference was found in the FA values between DTI and DSI ($P = 0.104$–0.391 [paired-samples t-test and Wilcoxon signed-rank test]).

Reproducibility of DTI and DSI

Most of the CV values for architecture characteristics and diffusion properties of the two scans were within the acceptable range (i.e., < 10%) in both DTI and DSI sequences, with the exception of the slight over-range in the T_N of the L-LPM (CV = 11.46%) and the QA of the R-LPM in DSI (CV = 10.50%) (Table 2).

Additionally, the RADs of the DTI- and DSI-derived metrics were relatively low (within ± 10%) (Table 2). However, significant relative differences were noted between the two scans, including in the T_N of the R-LPM (RAD = 6.50%) and T_V of the L-MM (RAD = 3.15%) in DTI, and T_N (RAD = 3.06%), MD (RAD = 2.99%), AD (RAD = 2.30%), and RD (RAD = 3.51%) of the L-MPM in DSI ($P < 0.05$ [paired-samples t-test]). No statistically significant relative differences were observed for the other metrics obtained by both diffusion models.

The Bland-Altman plots also showed satisfactory agreement between the two scans for all architecture characteristics and diffusion properties obtained with both DTI and DSI (Fig. 4). In most cases, the differences between the two measurements were within the limit of agreement. A representative case of the DTI and DSI fiber-tracking results between two scans is shown in Fig. 5.

Baseline characteristics of healthy volunteers and patients

Table S3 summarizes the baseline characteristics of patients and healthy controls. There were no significant differences in sex, age, and body mass index between the two groups (all $P > 0.05$ [Student's t-test, Mann-Whitney U test, Chi-square test]).

Sensitivity to microenvironment changes

Compared with the healthy volunteers, in LPMs, DTI showed that TMDs patients had lower T_V ($P = 0.010$ [Student's t-test]), RD ($P = 0.025$ [Student's t-test]), and increased FA ($P = 0.003$ [Mann-Whitney U test]). Whereas DSI, in addition to showing lower T_V ($P = 0.033$ [Student's t-test]) and RD ($P = 0.006$ [Student's t-test]), MD ($P = 0.005$ [Student's t-test]) and AD ($P = 0.006$ [Student's t-test]) were also found to be significantly lower in the TMDs group. In MMs, both DTI and DSI showed that TMDs patients had smaller T_V than healthy volunteers (DTI: $P = 0.011$ [Student's t-test]; DSI: $P = 0.004$ [Student's t-test]) and increased AD (DTI: $P = 0.009$ [Mann-Whitney U test]; DSI: $P = 0.016$ [Student's t-test]). Additionally, the DSI showed significant differences

Table 2 Variability, accuracy of consecutive DTI and DSI measurements

Tract name	Metrics	DTI				DSI			
		Scan 1 ($n=23$)	Scan 2 ($n=23$)	CV (%)	RAD (%)	Scan 1 ($n=23$)	Scan 2 ($n=23$)	CV (%)	RAD (%)
L-LPM	T_N ($\times10^3$)	6.15 ± 1.55	5.89 ± 1.22	5.49	3.32	22.85 ± 5.06	21.40 ± 5.88	**11.46**	7.19
	T_{ML} (mm)	21.98 [20.91, 23.01]	22.25 [20.15, 23.53]	3.50	-1.65	21.30 ± 3.07	20.10 ± 2.42	6.38	5.41
	T_V ($\times10^3$ mm^3)	12.30 [10.97, 14.49]	11.98 [11.02, 13.76]	4.61	1.93	12.99 [11.30, 13.69]	11.40 [10.36, 13.46]	9.62	7.51
	FA	0.27 ± 0.02	0.27 ± 0.02	3.90	-0.04	0.26 [0.25, 0.28]	0.26 [0.25, 0.28]	3.95	1.47
	MD ($\times10^{-3}$ mm^2/s)	1.71 ± 0.16	1.71 ± 0.22	4.57	0.71	2.33 ± 0.21	2.34 ± 0.29	4.23	0.10
	AD ($\times10^{-3}$ mm^2/s)	2.17 ± 0.20	2.16 ± 0.26	4.18	0.76	2.99 ± 0.25	2.98 ± 0.34	3.78	0.54
	RD ($\times10^{-3}$ mm^2/s)	1.49 ± 0.14	1.48 ± 0.20	4.92	0.68	2.01 ± 0.19	2.02 ± 0.27	4.64	-0.23
	QA	-	-	-	-	0.06 ± 0.01	0.06 ± 0.01	9.96	6.88
R-LPM	T_N ($\times10^3$)	6.47 ± 1.03	6.10 ± 1.19	5.91	**6.50**	24.04 ± 4.85	23.82 ± 6.69	9.83	3.62
	T_{ML} (mm)	23.89 ± 2.35	22.89 ± 2.30	4.21	4.29	21.85 ± 2.52	21.70 ± 3.35	5.34	1.16
	T_V ($\times10^3$ mm^3)	13.26 ± 2.15	12.86 ± 2.40	3.87	3.46	13.28 ± 2.75	12.43 ± 3.14	9.60	7.87
	FA	0.27 ± 0.02	0.27 ± 0.02	4.37	2.01	0.26 ± 0.02	0.26 ± 0.02	4.83	0.00
	MD ($\times10^{-3}$ mm^2/s)	1.71 ± 0.15	1.73 ± 0.17	2.83	-0.85	2.35 [2.22, 2.43]	2.27 [1.98, 2.49]	3.85	2.85
	AD ($\times10^{-3}$ mm^2/s)	2.18 ± 0.19	2.19 ± 0.20	2.50	-0.16	2.96 [2.83, 3.13]	2.96 [2.55, 3.18]	3.17	2.77
	RD ($\times10^{-3}$ mm^2/s)	1.47 ± 0.13	1.50 ± 0.16	3.18	-1.35	2.00 ± 0.20	1.94 ± 0.26	4.39	2.92
	QA	-	-	-	-	0.06 ± 0.01	0.05 ± 0.01	**10.50**	7.20
L-MM	T_N ($\times10^3$)	27.47 ± 6.14	26.75 ± 6.10	3.33	2.90	102.17 ± 20.07	102.40 ± 19.72	5.95	-0.30
	T_{ML} (mm)	30.43 ± 3.95	31.31 ± 4.68	4.80	-2.54	28.51 ± 4.81	28.23 ± 3.51	5.11	0.33
	T_V ($\times10^3$ mm^3)	45.79 ± 9.38	44.48 ± 9.44	2.76	**3.15**	40.90 ± 9.26	39.23 ± 9.30	5.45	4.51
	FA	0.27 ± 0.02	0.27 ± 0.02	2.48	0.46	0.27 ± 0.03	0.27 ± 0.02	3.84	-2.07
	MD ($\times10^{-3}$ mm^2/s)	1.60 ± 0.09	1.63 ± 0.13	3.01	-1.73	1.86 [1.74, 1.93]	1.75 [1.68, 1.91]	3.71	2.64
	AD ($\times10^{-3}$ mm^2/s)	2.06 ± 0.12	2.09 ± 0.15	2.80	-1.69	2.37 ± 0.15	2.32 ± 0.18	3.31	2.32
	RD ($\times10^{-3}$ mm^2/s)	1.37 ± 0.09	1.39 ± 0.12	3.47	-1.76	1.60 [1.46, 1.66]	1.47 [1.42, 1.66]	4.12	2.85
	QA					0.05 ± 0.01	0.05 ± 0.01	8.03	2.88
R-MM	T_N ($\times10^3$)	28.26 ± 6.06	27.55 ± 5.73	4.30	2.50	103.97 ± 23.53	103.57 ± 20.23	5.57	-0.21
	T_{ML} (mm)	35.17 [32.00, 36.97]	33.23 [31.08, 36.40]	5.14	1.42	31.62 ± 3.69	31.47 ± 4.26	4.00	0.68
	T_V ($\times10^3$ mm^3)	47.14 ± 8.75	46.17 ± 8.83	2.80	2.29	41.82 ± 8.72	40.48 ± 9.45	6.22	3.90
	FA	0.27 ± 0.02	0.28 ± 0.02	3.17	-1.34	0.26 ± 0.03	0.27 ± 0.03	3.34	-3.17
	MD ($\times10^{-3}$ mm^2/s)	1.59 ± 0.08	1.61 ± 0.13	2.33	-1.03	1.85 ± 0.15	1.82 ± 0.17	3.23	1.85
	AD ($\times10^{-3}$ mm^2/s)	2.05 ± 0.09	2.09 ± 0.15	2.19	-1.52	2.37 ± 0.15	2.35 ± 0.18	2.77	1.07
	RD ($\times10^{-3}$ mm^2/s)	1.36 ± 0.08	1.38 ± 0.12	2.61	-0.66	1.59 ± 0.15	1.55 ± 0.17	3.64	2.44
	QA	-	-	-	-	0.05 [0.04, 0.05]	0.04 [0.04, 0.05]	8.63	2.30
L-MPM	T_N ($\times10^3$)	8.26 ± 1.81	8.10 ± 2.29	6.94	4.37	31.06 ± 6.92	30.12 ± 6.65	7.34	**3.06**
	T_{ML} (mm)	24.61 ± 3.15	24.91 ± 3.92	5.88	-0.70	23.34 [21.72, 24.55]	22.25 [21.47, 24.07]	5.27	-1.62
	T_V ($\times10^3$ mm^3)	17.43 [15.75, 19.39]	17.50 [15.19, 20.65]	5.65	3.82	16.69 [15.06, 18.92]	15.18 [13.50, 18.90]	7.28	7.87
	FA	0.28 [0.28, 0.29]	0.28 [0.27, 0.29]	3.34	0.81	0.27 ± 0.02	0.27 ± 0.02	3.22	-1.99
	MD ($\times10^{-3}$ mm^2/s)	1.58 ± 0.09	1.59 ± 0.15	2.96	-0.33	1.99 ± 0.13	1.94 ± 0.17	2.57	**2.99**
	AD ($\times10^{-3}$ mm^2/s)	2.03 ± 0.13	2.04 ± 0.19	2.61	-0.20	2.55 ± 0.16	2.50 ± 0.19	2.13	**2.30**
	RD ($\times10^{-3}$ mm^2/s)	1.35 ± 0.08	1.36 ± 0.13	3.30	-0.42	1.72 ± 0.12	1.66 ± 0.15	3.03	**3.51**
	QA	-	-	-	-	0.05 ± 0.01	0.05 ± 0.01	7.45	4.50
R-MPM	T_N ($\times10^3$)	7.87 [7.02, 9.21]	7.70 [6.49, 9.04]	6.86	5.61	14.99 [13.36, 17.80]	14.38 [12.82, 18.43]	8.44	3.02
	T_{ML} (mm)	24.05 ± 3.73	24.33 ± 3.41	5.07	-1.35	22.08 ± 3.57	21.22 ± 2.99	6.07	3.49
	T_V ($\times10^3$ mm^3)	17.72 ± 3.51	17.12 ± 3.63	5.11	3.85	16.38 ± 4.84	15.78 ± 3.77	7.48	2.65
	FA	0.27 ± 0.02	0.27 ± 0.02	3.33	-0.09	0.26 ± 0.02	0.26 ± 0.02	3.90	-0.73
	MD ($\times10^{-3}$ mm^2/s)	1.60 ± 0.09	1.61 ± 0.15	3.35	-0.44	2.01 ± 0.17	1.97 ± 0.19	3.00	2.24
	AD ($\times10^{-3}$ mm^2/s)	2.05 ± 0.11	2.07 ± 0.17	3.12	-0.51	2.56 ± 0.20	2.51 ± 0.21	2.36	1.94
	RD ($\times10^{-3}$ mm^2/s)	1.38 ± 0.09	1.39 ± 0.14	3.57	-0.38	1.73 ± 0.15	1.69 ± 0.19	3.58	2.49
	QA	-	-	-	-	0.05 ± 0.01	0.05 ± 0.01	7.30	3.44

Note: L-LPM, left lateral pterygoid muscle; R-LPM, right lateral pterygoid muscle; L-MM, left masseter muscle; R-MM, right masseter muscle; L-MPM, left medial pterygoid muscle; R-MPM, right medial pterygoid muscle; T_N, track number; T_{ML}, track mean length; T_V, track volume; FA, fractional anisotropy; MD, mean diffusivity; AD, axial diffusivity; RD, radial diffusivity; QA, quantitative anisotropy; DTI, diffusion tensor imaging; DSI, diffusion spectral imaging; CV, coefficient of variation; RAD, relative absolute difference

Bold type indicated CV larger than 10% or statistically significant difference between RAD and zero

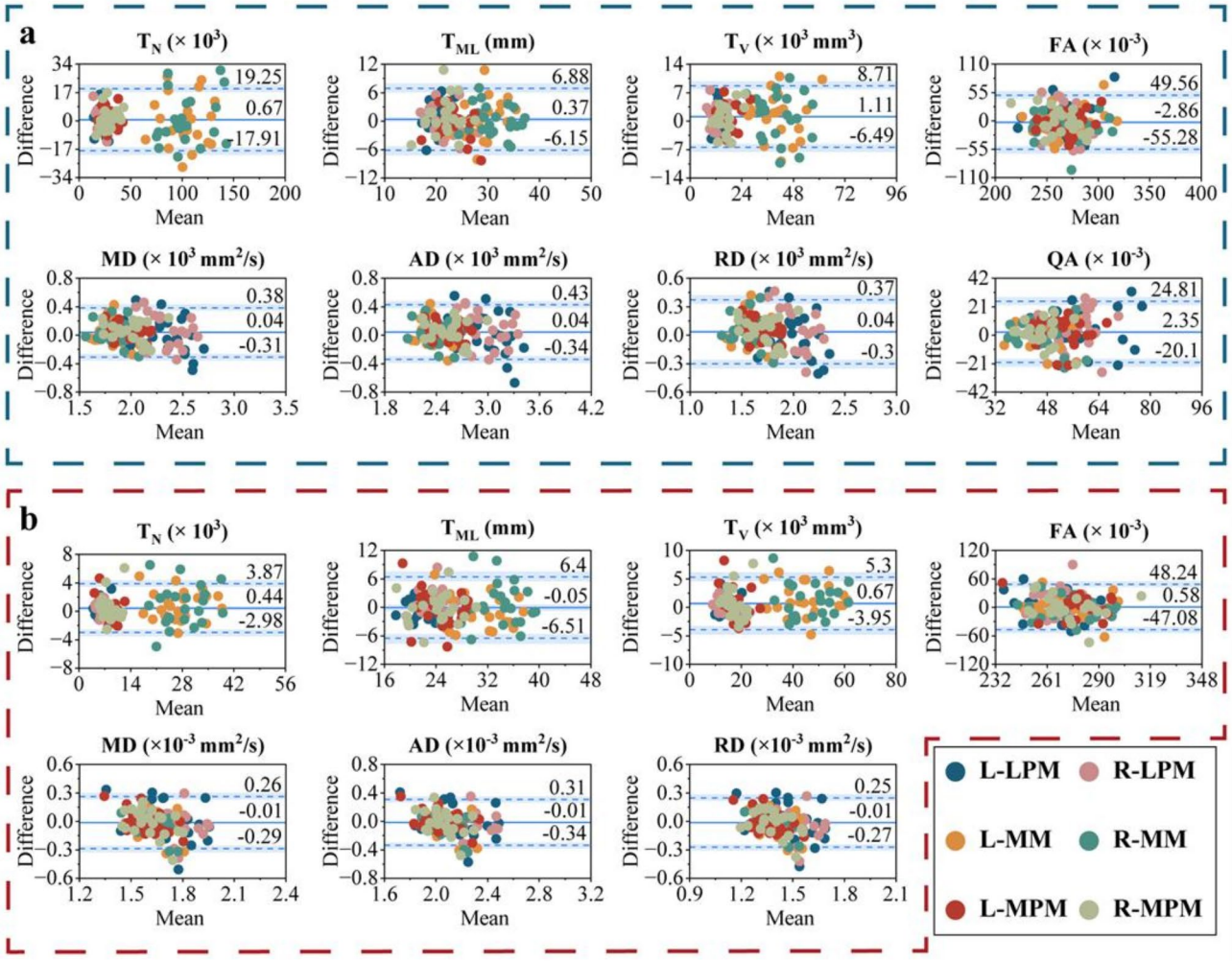

Fig. 4 Bland-Altman plots of the DSI-derived (**a**) and DTI-derived (**b**) diffusion properties and fiber-tracking metrics per muscle. The 95% confidence interval (limit of agreement) and the mean of the paired difference are indicated by dashed and solid blue lines, respectively. L-LPM, left lateral pterygoid muscle; R-LPM, right lateral pterygoid muscle; L-MM, left masseter muscle; R-MM, right masseter muscle; L-MPM, left medial pterygoid muscle; R-MPM, right medial pterygoid muscle; T_N, track number; T_{ML}, track mean length; T_V, track volume; FA, fractional anisotropy; MD, mean diffusivity; AD, axial diffusivity; RD, radial diffusivity; QA, quantitative anisotropy; DSI, diffusion spectral imaging; DTI, diffusion tensor imaging

in T_{ML} ($P = 0.002$ [Student's t-test]) and MD ($P = 0.040$ [Student's t-test]) between the TMDs patients and the healthy volunteers. Compared with healthy volunteers' MPMs, DTI ($P = 0.001$ [Mann-Whitney U test]) and DSI ($P < 0.001$ [Mann-Whitney U test]) found the decreasing T_V in TMDs patients. However, only DSI found significant differences in T_N ($P = 0.006$ [Student's t-test]), MD ($P = 0.043$ [Mann-Whitney U test]), and RD ($P = 0.040$ [Mann-Whitney U test]) of the MPMs between TMDs patients and healthy volunteers. (Table 3)

According to the status of disc displacement, the included 50 temporomandibular joints were further divided into three subgroups: NP ($n = 20$), ADWR ($n = 16$), and ADWOR ($n = 14$) (Table 4). There was no significant difference in any diffusion properties of DTI among TMDs subgroups, except for the smaller T_V in the ADWOR subgroup compared to the NP (LPMs: $P = 0.004$; MMs: $P = 0.009$ [one-way ANOVA followed *post-hoc* multiple comparisons]) and ADWR subgroups (LPMs: $P = 0.016$ [one-way ANOVA followed *post-hoc* multiple comparisons]) (Table 4; Fig. 6). For LPMs, DSI found significantly smaller T_V ($P = 0.036$ [one-way ANOVA followed *post-hoc* multiple comparisons]), lower QA ($P = 0.029$ [one-way ANOVA followed *post-hoc* multiple comparisons]), increased FA ($P = 0.010$ [one-way ANOVA followed *post-hoc* multiple comparisons]) in the ADWOR subgroup than ADWR subgroup, and smaller T_V in the ADWOR subgroup than the NP subgroup ($P = 0.019$ [one-way ANOVA followed *post-hoc* multiple comparisons]) (Table 4; Fig. 6). Smaller T_V of the MMs was also found by DSI in the ADWOR subgroup compared with the NP subgroup ($P = 0.011$ [one-way ANOVA

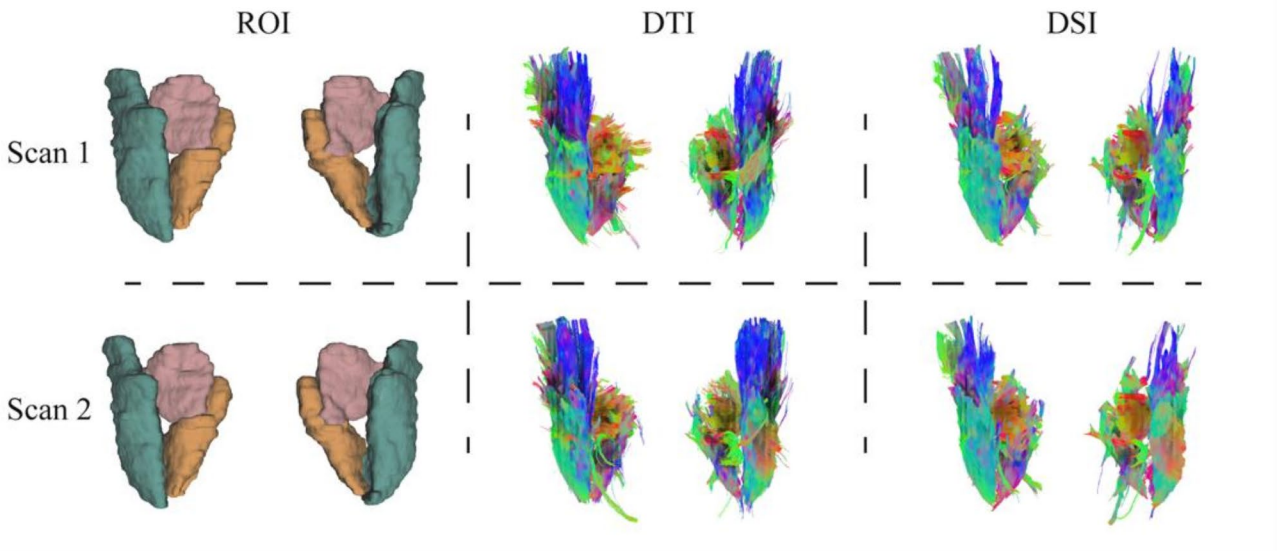

Fig. 5 Fiber tracking of the masticatory muscles on twice measurements with DTI and DSI. The tracking results of two scans of both DTI and DSI are similar, indicating satisfactory reproducibility. ROI, region of interest; DTI, diffusion tensor imaging; DSI, diffusion spectral imaging

followed *post-hoc* multiple comparisons]). In MPMs, DSI also detected smaller T_V in the ADWOR subgroup than in the ADWR ($P = 0.016$ [one-way ANOVA followed *post-hoc* multiple comparisons]) and NP ($P = 0.016$ [one-way ANOVA followed *post-hoc* multiple comparisons]) subgroups, which was not found by DTI (Table 4; Fig. 6).

Discussion

The present study aimed to evaluate and compare the performance of DTI and DSI in human masticatory muscles, in terms of differences, reproducibility, and sensitivity to muscular microenvironment changes. Although the results demonstrated both DTI and DSI allowed reproducible assessment of masticatory muscles, the quality of tracked fiber, architecture characteristics, and diffusion properties, was significantly different between them. And our results indicate that DSI could provide a more powerful ability to detect and quantify the changes in the muscular microenvironment in patients with TMDs.

It is increasingly recognized that incorrect fiber reconstructions are unavoidable during fiber tracking [28]. Our results suggest that DSI provides a more accurate depiction of the masticatory muscle fibers, as shown by a higher proportion of high-quality fibers and a lower percentage of low-quality fibers compared with DTI. These results are consistent with those of a previous study comparing the tracking accuracy of the motor and language tracts using DTI and DSI, which demonstrated that DSI provided significantly better performance in fiber-tracking [16]. The relatively small volume of the masticatory muscles, compared with other skeletal muscles, in conjunction with magnetic field inhomogeneity induced by the air cavities, increases the difficulty of microstructure imaging with DTI and DSI. The multiple b values and multi-directional diffusion encoding of DSI can directly reflect the fiber orientation without model assumptions or overfitting limitations [16, 29]. In addition, DSI fiber tracking is based on QA, which defines the fiber orientation at the individual fiber level, whereas DTI uses FA at the voxel level [30]. As a result, DSI fiber tracking reduces the influence of the partial volume effect, which can affect the fiber orientation distribution and generate false fibers [30, 31]. Given these advantages, DSI seems to offer greater reliability than conventional DTI for the imaging of skeletal muscle fiber bundles, especially in small muscles and under suboptimal imaging conditions.

The number of traced fibers significantly influences the accurate characterization of the overall muscle architectural properties, such as fiber length [32]. A smaller number of fibers may lead to larger errors in the characterization of the overall muscle architectural properties. Our results showed that DSI could track more masticatory muscle fibers than DTI. Significantly, DSI detected the changes of T_{ML} in the MMs for the TMDs patients, which were not found by DTI. Upon this view, DSI may lower the risk of incorrect representation of the global muscle architecture.

Additionally, DSI showed shorter T_{ML} and smaller T_V than DTI in MMs. A previous study reported that the fiber length decreased as the number of diffusion sampling directions increased [33], indicating that neighboring fibers may be misconnected as a single fiber and resulting in an overestimation of the fiber length by applying an imaging modality with a low diffusion direction resolution (e.g. DTI). And our results showed that DSI, rather than DTI, could depict the microscopy

Table 3 Comparison of architecture characteristics and diffusion properties between healthy volunteer and TMDs groups with DTI and DSI

Tract name	Metrics	DTI			DSI		
		HV ($n=50$)	TMDs ($n=50$)	*P*-value	HV ($n=50$)	TMDs ($n=50$)	*P*-value
LPM	T_N ($\times10^3$)	5.24 ± 1.08	4.91 ± 1.71	0.253 [c]	19.74 ± 4.80	18.85 ± 7.52	0.486 [c]
	T_{ML} (mm)	21.71 ± 2.17	21.17 ± 3 0.60	0.361 [c]	20.24 ± 2.83	21.10 ± 3.52	0.182 [c]
	T_V ($\times10^3$ mm^3)	10.43 ± 1.92	9.23 ± 2.56	**0.010[c]**	10.55 ± 2.16	9.46 ± 2.82	**0.033[c]**
	FA	0.27 [0.25, 0.28]	0.28 [0.26,0.30]	**0.003[d]**	0.26 [0.25, 0.28]	0.27 [0.25, 0.29]	0.216 [d]
	MD ($\times10^{-3}$ mm^2/s)	1.70 ± 0.15	1.65 ± 0.15	0.146 [c]	2.29 ± 0.22	2.16 ± 0.22	**0.005[c]**
	AD ($\times10^{-3}$ mm^2/s)	2.17 [1.97, 2.27]	2.10 [1.96, 2.25]	0.354 [d]	2.92 ± 0.26	2.77 ± 0.26	**0.006[c]**
	RD ($\times10^{-3}$ mm^2/s)	1.47 ± 0.13	1.41 ± 0.12	**0.025[c]**	1.97 ± 0.20	1.86 ± 0.21	**0.006[c]**
	QA	-	-	-	0.06 ± 0.01	0.05 ± 0.01	0.189 [c]
MM	T_N ($\times10^3$)	23.62 ± 5.74	23.09 ± 6.62	0.670 [c]	94.88 ± 21.09	87.86 ± 21.61	0.103 [c]
	T_{ML} (mm)	31.40 ± 4.34	31.68 ± 5.59	0.782 [c]	29.80 ± 4.49	32.65 ± 4.65	**0.002[c]**
	T_V ($\times10^3$ mm^3)	37.96 ± 8.45	33.55 ± 8.55	**0.011[c]**	36.40 ± 8.06	31.82 ± 7.56	**0.004[c]**
	FA	0.27 ± 0.02	0.28 ± 0.03	**0.027[c]**	0.26 ± 0.03	0.26 ± 0.02	0.841 [c]
	MD ($\times10^{-3}$ mm^2/s)	1.61 ± 0.09	1.65 ± 0.11	0.056 [c]	1.82 ± 0.15	1.88 ± 0.15	**0.040[c]**
	AD ($\times10^{-3}$ mm^2/s)	2.05 [1.99, 2.13]	2.14 [2.03, 2.24]	**0.009[d]**	2.33 ± 0.15	2.42 ± 0.18	**0.016[c]**
	RD ($\times10^{-3}$ mm^2/s)	1.38 ± 0.09	1.40 ± 0.10	0.236 [c]	1.56 ± 0.15	1.62 ± 0.14	0.073 [c]
	QA	-	-	-	0.05 ± 0.01	0.05 ± 0.01	0.426 [c]
MPM	T_N ($\times10^3$)	6.34 [5.61, 7.23]	6.36 [4.13, 7.38]	0.208 [d]	24.96 ± 6.03	21.55 ± 5.98	**0.006[c]**
	T_{ML} (mm)	22.60 [21.06, 24.96]	22.16 [20.58, 24.13]	0.168 [d]	21.34 ± 3.06	21.35 ± 3.61	0.979 [c]
	T_V ($\times10^3$ mm^3)	12.07 [10.82, 14.39]	10.61 [8.13, 12.79]	**0.001[d]**	12.19 [11.09, 13.93]	10.42 [8.46, 12.30]	**< 0.001[d]**
	FA	0.27 [0.25, 0.28]	0.28 [0.26, 0.29]	**0.026[d]**	0.26 ± 0.02	0.25 ± 0.02	0.099 [c]
	MD ($\times10^{-3}$ mm^2/s)	1.57 ± 0.10	1.59 ± 0.14	0.642 [c]	1.97 [1.86, 2.04]	2.03 [1.92, 2.13]	**0.043[d]**
	AD ($\times10^{-3}$ mm^2/s)	2.00 ± 0.14	2.05 ± 0.20	0.194 [c]	2.50 ± 0.18	2.57 ± 0.19	0.066 [c]
	RD ($\times10^{-3}$ mm^2/s)	1.36 [1.30, 1.42]	1.34 [1.28, 1.42]	0.530 [d]	1.68 [1.60, 1.78]	1.76 [1.65, 1.85]	**0.040[d]**
	QA	-	-	-	0.04 [0.04, 0.05]	0.04 [0.04, 0.05] 0.644 [d]	

Note: LPM, lateral pterygoid muscle; MM, masseter muscle; MPM, medial pterygoid muscle; T_N, track number; T_{ML}, track mean length; T_V, track volume; FA, fractional anisotropy; MD, mean diffusivity; AD, axial diffusivity; RD, radial diffusivity; QA, quantitative anisotropy; DTI, diffusion tensor imaging; DSI, diffusion spectral imaging; HV, healthy volunteer; TMDs, temporomandibular joint disorders

Bold type indicated $P<0.05$. The superscript letter "c" indicates the use of the Student's t-test, while the superscript letter "d" denotes the use of the Mann-Whitney U test

Table 4 Comparison of architecture characteristics and diffusion properties among TMDs subgroups with DTI and DSI

Tract name	Metrics	DTI				DSI			
		NP ($n=20$)	ADWR ($n=16$)	ADWOR ($n=14$)	*P*-value	NP ($n=20$)	ADWR ($n=16$)	ADWOR ($n=14$)	*P*-value
LPM	T_N ($\times10^3$)	5.51 [3.69, 6.71]	5.11 [4.09, 6.03]	3.84 [2.91, 5.17]	0.069 [f]	19.76 ± 9.20	19.00 ± 6.31	17.40 ± 6.31	0.672 [e]
	T_{ML} (mm)	21.69 [18.12, 24.33]	20.93 [20.04, 22.86]	20.31 [16.49, 23.69]	0.649 [f]	22.39 [17.99, 24.11]	21.83 [19.29, 23.29]	19.71 [17.25, 23.90]	0.662 [f]
	T_V ($\times10^3$ mm^3)	10.11 ± 2.77	9.56 ± 2.04	7.61 ± 2.12	**0.013[e]**	10.29 ± 2.93	9.89 ± 2.57	7.77 ± 2.33	**0.024[e]**
	FA	0.28 [0.26, 0.30]	0.28 [0.27, 0.29]	0.28 [0.26, 0.29]	0.849 [f]	0.27 ± 0.02	0.25 ± 0.02	0.28 ± 0.03	**0.018[e]**
	MD ($\times10^{-3}$ mm^2/s)	1.62 [1.46, 1.77]	1.64 [1.59, 1.73]	1.59 [1.54, 1.73]	0.588 [f]	2.16 ± 0.22	2.22 ± 0.24	2.09 ± 0.20	0.311 [e]
	AD ($\times10^{-3}$ mm^2/s)	2.02 [1.89, 2.30]	2.13 [2.03, 2.21]	2.06 [1.95, 2.22]	0.581 [f]	2.78 ± 0.27	2.82 ± 0.26	2.72 ± 0.25	0.561 [e]
	RD ($\times10^{-3}$ mm^2/s)	1.41 [1.25, 1.53]	1.41 [1.35, 1.49]	1.36 [1.33, 1.46]	0.455 [f]	1.86 ± 0.20	1.92 ± 0.23	1.78 ± 0.19	0.206 [e]
	QA	-	-	-	-	0.06 ± 0.01	0.06 ± 0.01	0.05 ± 0.01	**0.042[e]**
MM	T_N ($\times10^3$)	25.11 ± 7.19	23.52 ± 5.01	19.72 ± 6.50	0.059 [e]	91.32 ± 22.38	83.46 ± 17.99	87.94 ± 24.74	0.565 [e]
	T_{ML} (mm)	33.69 [26.92, 36.53]	32.99 [31.76, 34.81]	28.83 [24.97, 36.40]	0.460 [f]	34.10 [31.92, 36.88]	33.73 [30.08, 36.55]	31.37 [28.66, 34.05]	0.169 [f]
	T_V ($\times10^3$ mm^3)	37.33 ± 8.82	32.83 ± 6.61	28.96 ± 8.12	**0.015[e]**	34.76 ± 7.86	31.93 ± 7.09	27.48 ± 5.77	**0.019[e]**
	FA	0.28 ± 0.03	0.28 ± 0.02	0.27 ± 0.03	0.357 [e]	0.27 ± 0.02	0.26 ± 0.02	0.26 ± 0.02	0.139 [e]
	MD ($\times10^{-3}$ mm^2/s)	1.62 ± 0.11	1.64 ± 0.13	1.69 ± 0.09	0.200 [e]	1.86 ± 0.17	1.89 ± 0.16	1.90 ± 0.12	0.755 [e]
	AD ($\times10^{-3}$ mm^2/s)	2.12 ± 0.16	2.14 ± 0.16	2.19 ± 0.15	0.444 [e]	2.40 ± 0.21	2.43 ± 0.19	2.43 ± 0.16	0.905 [e]
	RD ($\times10^{-3}$ mm^2/s)	1.36 [1.30, 1.44]	1.39 [1.28, 1.51]	1.45 [1.43, 1.48]	0.075 [f]	1.60 [1.47, 1.70]	1.67 [1.51, 1.73]	1.65 [1.54, 1.68]	0.469 [f]
	QA	-	-	-	-	0.05 ± 0.01	0.05 ± 0.01	0.04 ± 0.01	0.053 [e]
MPM	T_N ($\times10^3$)	6.18 ± 2.28	6.33 ± 1.50	4.84 ± 2.24	0.102 [e]	21.51 ± 5.49	22.50 ± 5.57	20.51 ± 7.27	0.670 [e]
	T_{ML} (mm)	22.42 [17.70, 23.63]	22.72 [21.23, 24.65]	21.01 [16.46, 23.75]	0.253 [f]	21.40 ± 4.06	22.57 ± 2.31	19.90 ± 3.83	0.128 [e]
	T_V ($\times10^3$ mm^3)	11.34 ± 3.04	10.66 ± 2.43	8.99 ± 2.79	0.059 [e]	11.26 ± 2.48	11.27 ± 3.06	9.12 ± 2.27	**0.043[e]**
	FA	0.27 [0.26, 0.29]	0.28 [0.27, 0.29]	0.28 [0.26, 0.30]	0.630 [f]	0.25 ± 0.02	0.25 ± 0.02	0.25 ± 0.02	0.929 [e]
	MD ($\times10^{-3}$ mm^2/s)	1.54 ± 0.14	1.65 ± 0.15	1.58 ± 0.10	0.085 [e]	2.01 ± 0.18	2.06 ± 0.19	2.02 ± 0.14	0.696 [e]
	AD ($\times10^{-3}$ mm^2/s)	1.91 [1.84, 2.06]	2.09 [2.01, 2.29]	2.00 [1.88, 2.17]	0.054 [f]	2.51 [2.43, 2.62]	2.60 [2.41, 2.82]	2.55 [2.51, 2.70]	0.405 [f]
	RD ($\times10-3$ mm2/s)	1.32 ± 0.10	1.41 ± 0.13	1.35 ± 0.07	0.060 [e]	1.75 ± 0.16	1.79 ± 0.18	1.75 ± 0.14	0.748 [e]
	QA	-	-	-	-	0.04 ± 0.01	0.05 ± 0.01	0.04 ± 0.01	**0.049[e]**

Note: LPM, lateral pterygoid muscle; MM, masseter muscle; MPM, medial pterygoid muscle; T_N, track number; T_{ML}, track mean length; T_V, track volume; FA, fractional anisotropy; MD, mean diffusivity; AD, axial diffusivity; RD, radial diffusivity; QA, quantitative anisotropy; DTI, diffusion tensor imaging; DSI, diffusion spectral imaging; NP, normal disc position; ADWR, anterior disc displacement with reduction; ADWOR, anterior disc displacement without reduction

Bold type indicated $P<0.05$. The superscript letter "e" indicates the use of the one-way ANOVA, while the superscript letter "f" denotes the use of the Kruskal-Wallis test

change of T_V of MPMs among TMDs subgroups. TMDs may be associated with atrophy of masticatory muscle fibers [34, 35], resulting in smaller T_V. Thanks to the higher angle resolution and superior accuracy in fiber-tracking, DSI may be more sensitive to the change in architecture characteristics of masticatory muscle.

The diffusion properties (MD, AD, and RD) derived from DSI were significantly different from DTI in the present study. Diffusion properties correlate with the changes in muscle microstructure [36]. A prior study showed that the diffusion properties were significantly altered in the LPMs of patients with TMDs when compared with healthy volunteers. And the diffusion properties of LPMs also varied among different disc displacement statuses [13]. Consistent with this previous study, both DTI and DSI could depict the alteration of RD in LPMs and AD in MMs with TMDs. However, extra changes of the AD and MD in the LPMs, MD in the MMs, MD and RD in the MPMs were discovered with DSI in TMDs patients. It may indicate the results of DSI are more comprehensive and more consistent with the results of previous studies.

Our results showed that, compared to two other TMDs subgroups, the ADWOR group exhibited more

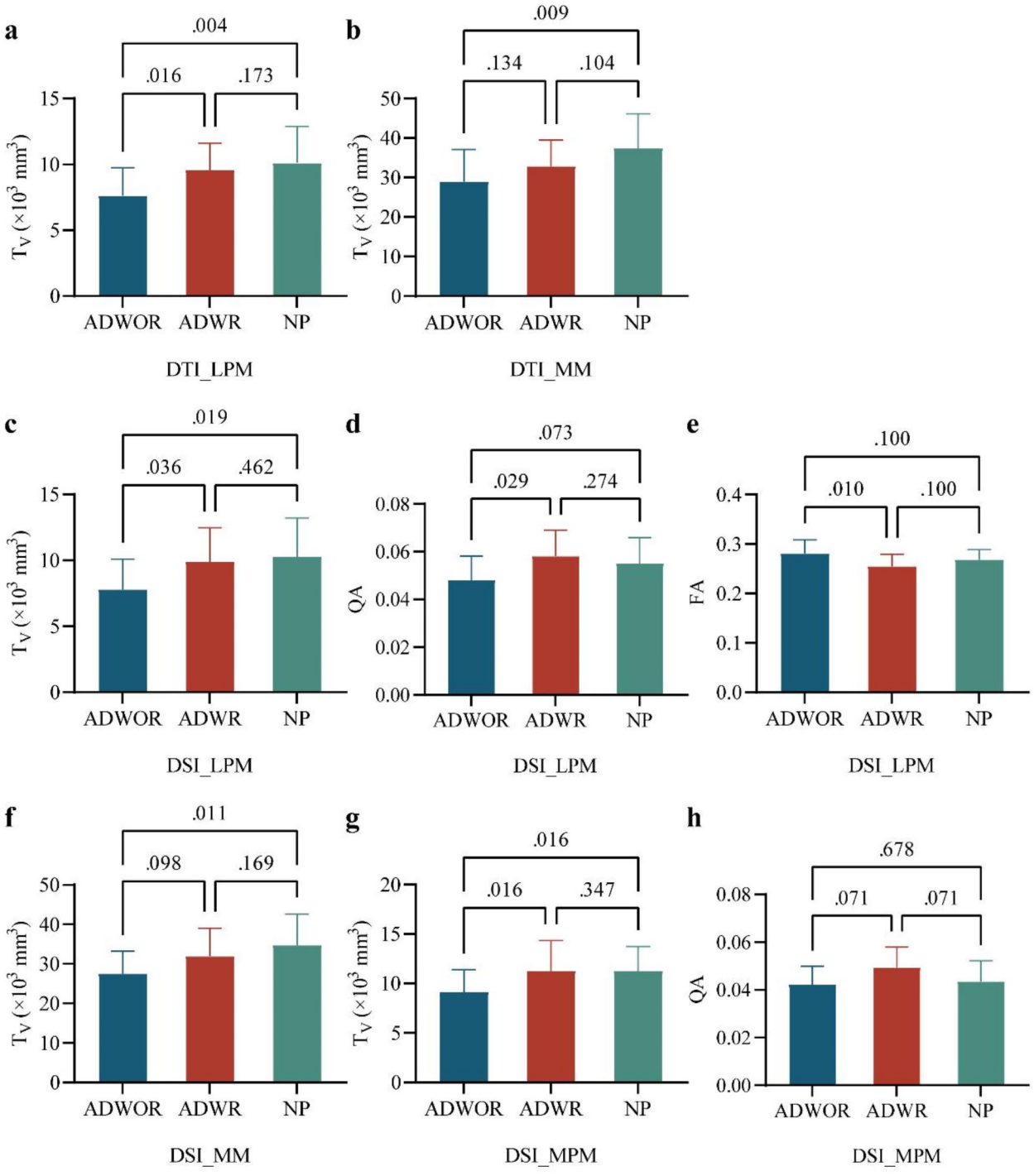

Fig. 6 Multiple comparisons of the architecture characteristics and diffusion properties among TMDs subgroups. TMDs, temporomandibular joint disorders; T_V, track volume; FA, fractional anisotropy; QA, quantitative anisotropy; NP, normal disc position; ADWR, anterior disc displacement with reduction; ADWOR, anterior disc displacement without reduction; DTI, diffusion tensor imaging; DSI, diffusion spectral imaging; LPM, lateral pterygoid muscle; MM, masseter muscle

pronounced changes in masticatory muscles, including smaller T_V, and lower QA and FA. The potential reasons may be that: (1) the changes in the masticatory muscles have been regarded as subsequent changes in the later stage of TMDs (ADWOR) rather than the early stage (NP and ADWR) [37]; the ADWOR status may lead to atrophy and fiber microstructure injury, which demonstrated as the decrease of T_V and increase in the QA and FA.

Most architecture characteristics and diffusion properties exhibited good reproducibility; however, a few metrics yielded relatively high variability for both DTI and DSI. The potential reasons for these variations may include (1) different scanning positions between the two sessions, possibly amplifying structural differences due to the limited spatial resolution (1.7 mm × 1.7 mm × 3 mm) and small muscle volumes, and (2) the influence of neighboring air on diffusion-weighted echo-planar imaging stability, despite standard corrections.

Limitations

This study has some limitations. First, the study population was relatively small. However, the satisfactory reproducibility and statistical performance of the comparison between DTI and DSI metrics supported our hypothesis. Therefore, this prospective and preliminary study can provide an essential reference basis for other researchers. In our future research, more samples will be included to strengthen our results. Another limitation is that the precise mechanisms underlying the different diffusion and fiber-tracking metrics between DTI and DSI have not been well clarified. However, our results suggested that DSI is more sensitive to the muscular microenvironment changes in masticatory muscle with TMDs, and previous studies on skeletal muscles of animals and the central nervous system have confirmed the superior performance of DSI compared to DTI [16, 22, 38]. Thirdly, TMDs may involve myogenic and arthrogenic etiologies. Relying solely on disc position for patient classification may represent an oversimplification, as it fails to account for potential confounding effects from other etiological factors on masticatory muscles. Future works should incorporate standard TMDs diagnostic protocols to better elucidate the intrinsic pathological mechanisms underlying masticatory muscle alterations. Finally, the scanning time of DSI is almost double that of DTI. And the relatively complex post-precessing process also impedes the wide clinical application of it. Therefore, accelerated MRI acquisition techniques (e.g. simultaneous multi-slice imaging), and more convenient and fast post-precessing software are urgently needed in the future to promote subsequent research and clinical applications.

Conclusions

In conclusion, although both DTI and DSI allow reproducible assessment of masticatory muscles, the architecture characteristics and diffusion properties were significantly different between them. DSI could provide a more powerful ability to detect and quantify the muscular microenvironment changes of masticatory muscles in patients with TMDs.

Abbreviations

AD	Axial diffusivity
ADWOR	Anterior disc displacement without reduction
ADWR	Anterior disc displacement with reduction
CV	Coefficient of variation
DSI	Diffusion spectrum imaging
DTI	Diffusion tensor imaging
FA	Fractional anisotropy
LPMs	Lateral pterygoid muscles
MD	Mean diffusivity
MMs	Masseter muscles
MPMs	Medial pterygoid muscles
MRI	Magnetic resonance imaging
NP	Normal disc position
QA	Quantitative anisotropy
RAD	Relative absolute difference
RD	Radial diffusivity
TMDs	Temporomandibular joint disorders
TML/n	Track mean length
TN/n	Track number
TV	Track volume

Supplementary Information

The online version contains supplementary material available at https://doi.org/10.1186/s12891-025-08635-7.

Supplementary Material 1

Supplementary Material 2

Supplementary Material 3

Acknowledgements

The authors declare that they have no known competing financial interests or personal relationships that could have appeared to influence the work reported in this paper.

Author contributions

Xiang Lin and Wei Guo: Conceptualization, Data curation, Formal Analysis, Funding acquisition, Investigation, Methodology, Visualization, Writing– original draft.Dejun She: Conceptualization, Methodology, Writing– review & editing.Jianping Hu: Methodology, Software.Hongpeng Dai: Investigation. Yang Song: Formal Analysis.Dairong Cao: Supervision, Investigation, Writing– review & editing.

Funding

This study has received funding from the Startup Fund for Scientific Research of Fujian Medical University (No.2022QH1101), and Joint Funds for the Innovation of Science and Technology, Fujian Province (No.2021Y9122).

Data availability

No datasets were generated or analysed during the current study.

Declarations

Ethics approval and consent to participate

This prospective study was approved by the Institutional Review Board of the First Affiliated Hospital of Fujian Medical University (MRCTA, ECFAH of FMU [2021] 674), and written informed consent was obtained from each participant. The authors confirm that all methods were performed in accordance with the Declaration of Helsinki and Ethical Review Methods for Biomedical Research on Human Beings.

Consent for publication

Not applicable.

Competing interests

Yang Song is an employee of Siemens Healthineers. The authors declare no other competing interests.

Author details
[1]Department of Radiology, the First Affiliated Hospital, Fujian Medical University, 20 Cha-Zhong Road, Fuzhou, Fujian 350005, China
[2]Department of Radiology, National Regional Medical Center, Binhai Campus of the First Affiliated Hospital, Fujian Medical University, Fuzhou 350212, China
[3]MR Scientific Marketing, Healthineers Ltd, Siemens, Shanghai 201318, China
[4]Department of Radiology, Fujian Key Laboratory of Precision Medicine for Cancer, The First Affiliated Hospital, Fujian Medical University, Fuzhou, Fujian 350005, China
[5]Key Laboratory of Radiation Biology of Fujian Higher Education Institutions, The First Affiliated Hospital, Fujian Medical University, Fuzhou, Fujian 350005, China

Received: 7 July 2024 / Accepted: 9 April 2025
Published online: 24 April 2025

References

1. Basit H, Tariq MA, Siccardi MA. Anatomy, Head and Neck, Mastication Muscles. In: *StatPearls [Internet]*. edn. Edited by Siccardi MA. Treasure Island, FL: StatPearls Publishing; 2023.
2. El Haddioui A, Laison F, Zouaoui A, Bravetti P, Gaudy JF. Functional anatomy of the human lateral pterygoid muscle. Surg Radiol Anat. 2005;27(4):271–86.
3. Gaudy JF, Zouaoui A, Bravetti P, Charrier JL, Guettaf A. Functional organization of the human masseter muscle. Surg Radiol Anat. 2000;22(3–4):181–90.
4. Botticchio A, Mourad F, Fernández-Carnero S, Arias-Buría JL, Santodomingo Bueno A, Mesa Jiménez J, Gobbo M. Short-Term morphological changes in asymptomatic perimandibular muscles after dry needling assessed with rehabilitative ultrasound imaging: A Proof-of-Concept study. J Clin Med. 2021;10(2).
5. Moayedi M, Krishnamoorthy G, He P-YT, Agur A, Weissman-Fogel I, Tenenbaum HC, Lam EWN, Davis KD, Henderson L, Cioffi I. Structural abnormalities in the temporalis musculo-aponeurotic complex in chronic muscular temporomandibular disorders. Pain. 2020;161(8):1787–97.
6. Zieliński G, Pająk-Zielińska B, Ginszt M. A Meta-Analysis of the global prevalence of temporomandibular disorders. J Clin Med. 2024;13(5).
7. List T, Jensen RH. Temporomandibular disorders: old ideas and new concepts. Cephalalgia. 2017;37(7):692–704.
8. Penlington C, Bowes C, Taylor G, Otemade AA, Waterhouse P, Durham J, Ohrbach R. Psychological therapies for temporomandibular disorders (TMDs). Cochrane Database Syst Rev. 2022;8(8):CD013515.
9. Gatchel RJ, Stowell AW, Wildenstein L, Riggs R, Ellis E. Efficacy of an early intervention for patients with acute temporomandibular disorder-related pain: a one-year outcome study. J Am Dent Assoc. 2006;137(3):339–47.
10. Yıldız NT, Kocaman H, Yıldırım H, Canlı M. An investigation of machine learning algorithms for prediction of temporomandibular disorders by using clinical parameters. Med (Baltim). 2024;103(41):e39912.
11. Schiffman E, Ohrbach R, Truelove E, Look J, Anderson G, Goulet J-P, List T, Svensson P, Gonzalez Y, Lobbezoo F et al. Diagnostic criteria for temporomandibular disorders (DC/TMD) for clinical and research applications: recommendations of the international RDC/TMD consortium network** and orofacial pain special interest group†. J Oral Facial Pain Headache 2014;28(1).
12. Xiong X, Ye Z, Tang H, Wei Y, Nie L, Wei X, Liu Y, Song B. MRI of temporomandibular joint disorders: recent advances and future directions. J Magn Reson Imaging. 2021;54(4):1039–52.
13. Liu S, Wan C, Li H, Chen W, Pan C. Diffusion tensor imaging of the lateral pterygoid muscle in patients with temporomandibular joint disorders and healthy volunteers. Korean J Radiol. 2022;23(2):218–25.
14. Shiraishi T, Chikui T, Inadomi D, Kagawa T, Yoshiura K, Yuasa K. Evaluation of diffusion parameters and T2 values of the masseter muscle during jaw opening, clenching, and rest. Acta Radiol. 2012;53(1):81–6.
15. Ha D-H, Choi S, Kang E-J, Park HT. Diffusion tensor imaging and T2 mapping in early denervated skeletal muscle in rats. J Magn Reson Imaging. 2015;42(3):617–23.
16. Young RJ, Tan ET, Peck KK, Jenabi M, Karimi S, Brennan N, Rubel J, Lyo J, Shi W, Zhang Z, et al. Comparison of compressed sensing diffusion spectrum imaging and diffusion tensor imaging in patients with intracranial masses. Magn Reson Imaging. 2017;36:24–31.
17. Chung HW, Chou MC, Chen CY. Principles and limitations of computational algorithms in clinical diffusion tensor MR tractography. AJNR Am J Neuroradiol. 2011;32(1):3–13.
18. Oouchi H, Yamada K, Sakai K, Kizu O, Kubota T, Ito H, Nishimura T. Diffusion anisotropy measurement of brain white matter is affected by voxel size: underestimation occurs in areas with crossing fibers. AJNR Am J Neuroradiol. 2007;28(6):1102–6.
19. Wedeen VJ, Wang RP, Schmahmann JD, Benner T, Tseng WYI, Dai G, Pandya DN, Hagmann P, D'Arceuil H, de Crespigny AJ. Diffusion spectrum magnetic resonance imaging (DSI) tractography of crossing fibers. NeuroImage. 2008;41(4):1267–77.
20. Wang TT, Kwon HS, Dai G, Wang R, Mijailovich SM, Moss RL, So PTC, Wedeen VJ, Gilbert RJ. Resolving myoarchitectural disarray in the mouse ventricular wall with diffusion spectrum magnetic resonance imaging. Ann Biomed Eng. 2010;38(9):2841–50.
21. Ye C, Murano E, Stone M, Prince JL. A bayesian approach to distinguishing interdigitated tongue muscles from limited diffusion magnetic resonance imaging. Comput Med Imaging Graph. 2015;45:63–74.
22. Gilbert RJ, Magnusson LH, Napadow VJ, Benner T, Wang R, Wedeen VJ. Mapping complex myoarchitecture in the bovine tongue with diffusion-spectrum magnetic resonance imaging. Biophys J. 2006;91(3):1014–22.
23. Schiffman E, Ohrbach R, Truelove E, Look J, Anderson G, Goulet J-P, List T, Svensson P, Gonzalez Y, Lobbezoo F, et al. Diagnostic criteria for temporomandibular disorders (DC/TMD) for clinical and research applications: recommendations of the international RDC/TMD consortium network** and orofacial pain special interest group†. J Oral Facial Pain Headache. 2014;28(1):6–27.
24. Sugano T, Ogawa T, Yoda N, Hashimoto T, Shobara K, Niizuma K, Kawashima R, Sasaki K. Morphological comparison of masseter muscle fibres in the mandibular rest and open positions using diffusion tensor imaging. J Oral Rehabil. 2022;49(6):608–15.
25. Heemskerk AM, Sinha TK, Wilson KJ, Ding Z, Damon BM. Quantitative assessment of DTI-based muscle fiber tracking and optimal tracking parameters. Magn Reson Med. 2009;61(2):467–72.
26. Giraudo C, Motyka S, Weber M, Feiweier T, Trattnig S, Bogner W. Diffusion tensor imaging of healthy skeletal muscles: A comparison between 7 T and 3 T. Invest Radiol. 2019;54(1):48–54.
27. Vargas HA, Kramer GM, Scott AM, Weickhardt A, Meier AA, Parada N, Beattie BJ, Humm JL, Staton KD, Zanzonico PB, et al. Reproducibility and repeatability of semiquantitative 18F-Fluorodihydrotestosterone uptake metrics in Castration-Resistant prostate Cancer metastases: A prospective multicenter study. J Nucl Med. 2018;59(10):1516–23.
28. Maier-Hein KH, Neher PF, Houde J-C, Côté M-A, Garyfallidis E, Zhong J, Chamberland M, Yeh F-C, Lin Y-C, Ji Q, et al. The challenge of mapping the human connectome based on diffusion tractography. Nat Commun. 2017;8(1):1349.
29. Wedeen VJ, Hagmann P, Tseng W-YI, Reese TG, Weisskoff RM. Mapping complex tissue architecture with diffusion spectrum magnetic resonance imaging. Magn Reson Med. 2005;54(6):1377–86.
30. Yeh F-C, Wedeen VJ, Tseng W-YI. Generalized q-sampling imaging. IEEE Trans Med Imaging. 2010;29(9):1626–35.
31. Yeh F-C, Tseng W-YI. Sparse solution of fiber orientation distribution function by diffusion decomposition. PLoS ONE. 2013;8(10):e75747.
32. Charles J, Kissane R, Hoehfurtner T, Bates KT. From fibre to function: are we accurately representing muscle architecture and performance? Biol Rev Camb Philos Soc. 2022;97(4):1640–76.
33. Sugano T, Yoda N, Ogawa T, Hashimoto T, Shobara K, Niizuma K, Kawashima R, Sasaki K. Application of diffusion tensor imaging Fiber tractography for human masseter muscle. Tohoku J Exp Med. 2022;256(2):151–60.
34. D'Ippolito SM, Borri Wolosker AM, D'Ippolito G, de Herbert B, Fenyo-Pereira M. Evaluation of the lateral pterygoid muscle using magnetic resonance imaging. Dentomaxillofac Radiol. 2010;39(8):494–500.
35. Scrivani SJ, Keith DA, Kaban LB. Temporomandibular disorders. N Engl J Med. 2008;359(25):2693–705.
36. Oudeman J, Nederveen AJ, Strijkers GJ, Maas M, Luijten PR, Froeling M. Techniques and applications of skeletal muscle diffusion tensor imaging: A review. J Magn Reson Imaging. 2016;43(4):773–88.
37. Butts R, Dunning J, Perreault T, Mettille J, Escaloni J. Pathoanatomical characteristics of temporomandibular dysfunction: where do we stand? (Narrative review part 1). J Bodyw Mov Ther. 2017;21(3):534–40.

38. Jones R, Maffei C, Augustinack J, Fischl B, Wang H, Bilgic B, Yendiki A. High-fidelity approximation of grid- and shell-based sampling schemes from undersampled DSI using compressed sensing: post mortem validation. NeuroImage. 2021;244:118621.

Publisher's note